Engineering Geology 181 (2014) 202–211

Contents lists available at ScienceDirect

Engineering Geology

journal homepage: www.elsevier.com/locate/enggeo

Development and application of a pseudo-3D pit slope displacement map derived from ground-based radar

J. Severin [a,b,*], E. Eberhardt [b], L. Leoni [c], S. Fortin [d]

[a] SRK Consulting (Canada) Inc., Suite 2200, 1066 West Hastings St., Vancouver V6E 3X2, Canada
[b] Geological Engineering, Dept. of Earth, Ocean & Atmospheric Sciences, University of British Columbia, Vancouver, BC, Canada
[c] IDS Ingegneria Dei Sistemi, GeoRadar Division, Pisa, Italy
[d] Teck Highland Valley Copper, Logan Lake, BC, Canada

ARTICLE INFO

Article history:
Received 17 February 2014
Received in revised form 17 July 2014
Accepted 20 July 2014
Available online 28 July 2014

Keywords:
Rock slope monitoring
Ground based synthetic aperture radar
Rock slope kinematics
Open pit mining

ABSTRACT

Slope monitoring plays an important role in the risk management of large open pit slopes. Historically, displacement data derived from measuring geodetic prisms have been relied upon to delineate the boundaries of potential slope hazards; however that data can be limited by its point-measurement nature. Localized displacements at each prism may be misinterpreted when extended to the behavior of the entire slope, and important displacements between prisms may be overlooked. New technologies like ground-based radar can provide high resolution, full area coverage of a slope in combination with near real-time acquisition and millimeter precision. As a line-of-sight instrument, these tools provide data on displacement magnitudes and rates, but not true direction hence limiting their use in gaining understanding of the kinematics and behavior of the moving slope. This paper describes a novel experiment in which two ground-based synthetic aperture radar systems were simultaneously deployed to record continuous, line-of-sight displacements of an open pit slope in "stereo". The displacement vectors were combined to create a pseudo 3-D displacement map for the slope, which was subsequently used to interpret the influence of a major fault and the rock mass fabric in promoting different kinematic responses. The data collected demonstrates that an improved understanding of the 3-D kinematics of a large rock slope can be achieved using advanced state-of-the-art monitoring techniques to aid mine design.

1. Introduction

Slope monitoring through the use of radar, geodetic prisms, visual observations, and other geotechnical instruments forms a key component of modern open pit slope management programs for a majority of mining companies. The management programs are designed to focus on providing an early warning of an impending slope failure so that personal risk to mining staff is minimized while mine production is maximized by reducing downtime of the mine. Standard slope monitoring practices typically involve the periodic measurement of geodetic prisms by a survey crew or robotic total station to identify and quantify the nature and extent of pit slope movements. The prism data, being point measurements, are susceptible to uncertainty relating to the geological conditions and slope kinematics controlling the instability mechanism. The detection of accelerating behavior may either be an early warning of impending failure or a false alarm related to highly localized movements in the immediate vicinity of the prism. Similarly, the interpolation of slope behavior between prism locations may result in displacements influenced by large-scale geological structures being misinterpreted or missed all together. Increasingly, the geodetic data is collected in collaboration with radar instruments to help delineate the region of increased slope displacement and collect data between the geodetic prisms on the slope. Radar data is collected near continuously in real time, which creates a massive amount of data over a short period of time. As a result, it is often only used for early warning monitoring using vendor-provided software, even though it also contains useful information on the slope instability kinematics.

This paper outlines a novel experiment which may be repeated in cases where mine staff are required to investigate and gain a better understanding of the 3-D kinematics and dynamics of pit slope displacements which have been identified as representing a threat to mine operations and safety. The experiment involves the simultaneous deployment of two ground-based interferometric synthetic aperture radar systems which were used to collect continuous, line of sight displacement data in "stereo" of a large, moving open pit slope bisected by a large fault. The data and results presented demonstrate that an improved understanding of the 3-D kinematics of the slope and influence of large scale geological structures can be achieved using advanced state-of-the-art monitoring techniques. This understanding can be

* Corresponding author at: Suite 2200, 1066 West Hastings St., Vancouver, BC V6E 3X2, Canada. Tel.: +1 604 681 4196, +1 604 368 5913 (mobile), +1 604 235 8518 (direct); fax: +1 604 687 5532.
E-mail addresses: jseverin@srk.com (J. Severin), erik@eos.ubc.ca (E. Eberhardt), l.leoni@idscorporation.com (L. Leoni), Sebastien.Fortin@teck.com (S. Fortin).

http://dx.doi.org/10.1016/j.enggeo.2014.07.016
0013-7952/

used to help mitigate the current risk presented by a slope or be used to design the next phase of an open pit layout (e.g. pushback).

2. Slope monitoring techniques

2.1. Investigative monitoring

For slope monitoring to be most effective, the data should first be used to gain a baseline understanding of the slope behavior before using it for predictive purposes and defining early warning alarm thresholds. Thus the function of the monitoring network can be seen as serving two purposes (Moore et al., 1991):

(i) Investigative monitoring: To provide an understanding of the slope behavior over time and typical responses to external events (e.g. precipitation and seasonal fluctuations).
(ii) Predictive monitoring: To provide a warning of a change in behavior, enabling the possibility of limiting damage or intervening to prevent hazardous sliding.

Investigative monitoring has been shown to facilitate a greater understanding of the behavior of both natural (Willenberg et al., 2008) and engineered slopes (Walker et al., 2006), thus enabling the correct mitigation measures to be selected or to confirm that the slope is performing as designed. Ultimately, pit slope monitoring is carried out to ensure the safety of workers and equipment. Alarm thresholds are usually set based on experience, extrapolating measured displacement-time series to detect accelerations that exceed set thresholds. Rose and Hungr (2007) demonstrated further utility by extrapolating the inverse velocity time series introduced by Fukuzono (1985). It must be noted that these approaches are generally applied independent of the failure mechanism or monitoring method (e.g., geodetic point measurement and tension crack opening). As such, false alarms or uncertainty over misleading instrument readings is a frequent problem. Once an alarm is triggered, the mine may shut down operations in the area of potential instability. If a failure occurs, the procedure is deemed a success (Day and Seery, 2007); if not, the procedure results in costly downtime, delays to production schedules and diminished confidence in the system.

2.2. Geodetic monitoring

Geodetic monitoring represents the most common method employed in pit slope management due to its general reliability, relative low cost, and ease of execution. The geodetic monitoring of numerous prisms installed on multiple benches is now routinely undertaken using robotic total stations, with recent efforts to combine these systems with global navigation satellite systems (Brown et al., 2007). Monitoring through GPS receivers has also been seen as an answer to large open pit projects where the pit diameter exceeds 1 km and refraction and pointing errors start to limit the effectiveness of total station measurements.

Outside of potential safety concerns during the deployment of the prisms, an important limitation of data collected from geodetic monitoring is that movement and deformations between prisms must be interpolated. This may result in: i) the boundaries of areas with high displacement rates being poorly defined, ii) smaller scale structurally controlled movements such as wedge or planar sliding to be overlooked, and/or iii) the kinematics behind larger and more complex pit-scale failures being misinterpreted.

2.3. Radar monitoring

New developments in slope monitoring include the use of remote sensing technologies like terrestrial radar, which provide high-resolution, full area spatial coverage as opposed to relying on geodetic point measurements. Radar works by continuously scanning and comparing highly accurate and precise measurements made from up to 4 km from the slope face to detect sub-millimeter movements (with an accuracy of 0.1 to 1 mm, depending on distance). Radar units can collect real-time, near-continuous (5 minute interval), line-of-sight (1-D) monitoring data of large areas in all weather conditions (Farina et al., 2012). Such capabilities are helping to establish radar as a key tool for managing unstable pit slopes, quickly identifying the size, extent and temporal behavior of a developing failure (e.g., Harries et al., 2006; Day and Seery, 2007; Harries and Roberts, 2007). Rödelsperger et al. (2010) describe the advantages and disadvantages of radar data as compared to other forms of monitoring. The precise measurement of displacement from far distances allows radar data to be used by researchers in several state of the art applications such as monitoring volcanic activity (Di Traglia et al., 2014), concrete dam displacement (Talich et al., 2014), and natural slope stability (Martino and Mazzanti, 2014).

Ground based synthetic aperture radar was initially applied to measurement of natural slope movements with the Italian Alps (Tarchi et al., 2003) in 2000 and since has been validated during multiple investigations of landslides (Noferini et al., 2007; Monserrat et al., 2013) and has been used as a predictive tool to forecast slope displacement (Herrera et al., 2009; Casagli et al, 2010).

One key limitation of all radar systems is that it can only provide line-of-sight displacement meaning that important 3-D information of the displacement kinematics may be missed.

The collection of large amounts of data in combination with a shrinking and overly specialized work force has had the unintended effect of reducing the mine geotechnical engineer to either a radar system trouble shooter or a data archive manager.

3. Full spatial detection of a slope

3.1. Teck Highland Valley Copper mine

The Teck Highland Valley Copper (THVC) mine is located near Kamloops in south-western British Columbia, Canada (Figure 1). THVC is a truck and shovel operation comprised of several open pits. The experiment described within this paper was carried out in the Lornex Pit.

The west wall of the Lornex Pit is a 400 m high slope with an overall angle of 29° (Figure 2). The rock is relatively competent but is altered in the vicinity of the fault zones. The west wall is bisected by the Lornex Fault Zone (LFZ), a zone of highly fractured and intensely altered rock ranging between 40 and 80 m that dips approximately 75° into the slope. The LFZ in conjunction with the other faults in the slope is interpreted as playing a critical role in controlling the kinematics of the upper slope movement (Rose and Scholz, 2009).

Other moderately to steeply dipping faults that trend northeast–southwest occur intermittently throughout the hanging wall of the LFZ. Movement within the hanging wall of the LFZ (upper slope) is reported as being caused by a complex toppling mechanism with a historical maximum daily velocity of greater than 300 mm/day (Rose and Scholz, 2009). At the time of the writing of this paper, the west wall of the Lornex Pit was well instrumented with over 75 geodetic prisms installed; however, the northwest portion of the pit wall is relatively void of prisms (Figure 3, left), primarily because of safety concerns, lack of access preventing their installation, or slope displacements that rendered them inoperative. The Lornex Pit is currently undergoing a pushback around its entire circumference.

3.2. Experiment set-up and instrument positioning

The radar system used in this study was an IBIS-M (manufactured by IDS Ingegneria Dei Sistemi). The system is based on: i) Stepped Frequency Continuous Wave (SF-CW), allowing resolution in the range direction, ii) Synthetic Aperture Radar (SAR), allowing the system to resolve the monitored region in the cross range direction, and iii) differential interferometry, which allows the measurement of displacements

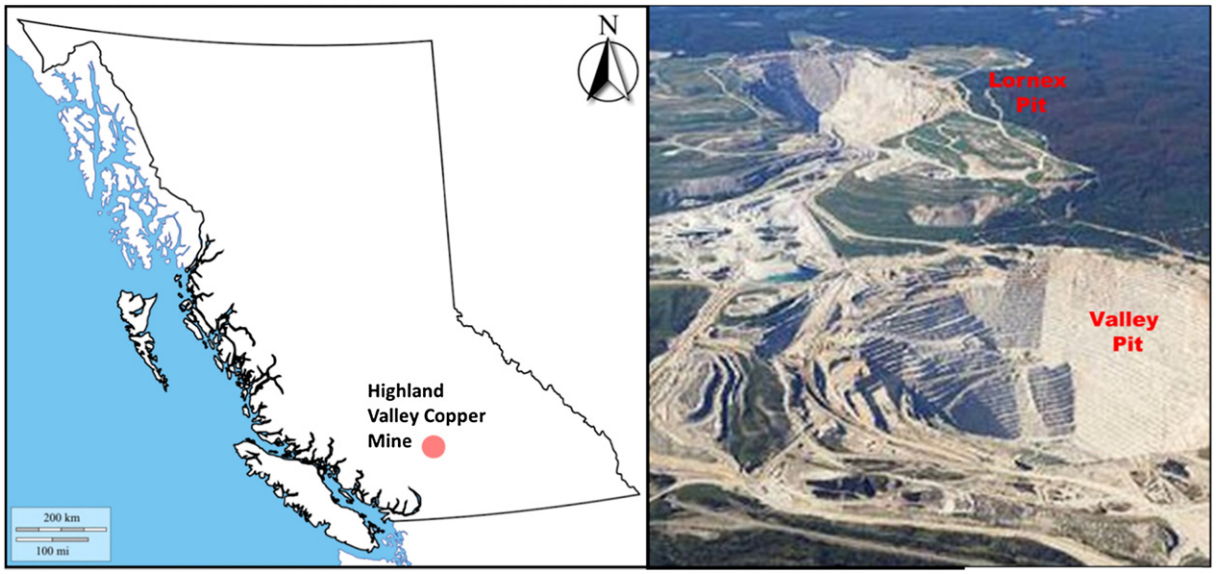

Fig. 1. Geographic location of study site, Teck Highland Valley Copper mine (left) with aerial view of Lornex and Valley Pits (right).

by comparing phase information of the back scattered electromagnetic waves collected at different times. The first radar unit (Site A) was located near the top of the northeast pit wall (Figure 3, right). The distance of the monitored points here ranged between approximately 800 and 1500 m. At this distance, the resolution of the monitored pixels was 1.5×4.3 m. This site was chosen for being roughly parallel to the general direction of slope movement. Site B was located at the top of the southeast pit wall, providing good spatial overlap with Site A and an oblique angle to the projected direction of slope movement. The distance of the monitored points ranged between 1200 and 2500 m, which correlates to a monitored pixel size of 1.5×8.6 m. Both monitoring sites were selected as their locations were stable (minimal displacement) and outside the range of any fly-rock generated from production blasts in the pit. Power to the radar units was provided by batteries and a portable power generator. The timing of the data collection scans was set to collect data simultaneously within the internal clock of the radar units with scan time intervals of approximately 6 min. The data was then collected for a 5 day overlap time. As the distances between the monitoring point and the wall of interest were different, the frequencies used to collect the data were not the same and no interference occurred. A typical radar setup is shown in Fig. 4. A full description of the IBIS-M system is given by Farina et al. (2012).

4. Data analysis

4.1. Resolving 3-D displacement vectors

The monitoring data was collected and processed using the software IBIS Controller® and IBIS Guardian® to remove the atmospheric artifacts, in both range and cross-range, from the phase information with a mathematical algorithm that is able to automatically discern stable points from those that are moving. This avoids the need to manually select ground control points. Two independent displacement maps in raster format for each of the installation points were created over the selected time frame. Using ArcGIS, the raster data set was combined with a digital elevation model (DEM) of the mine site and converted into global coordinates with displacement values. The slope was pixelated into a grid of between 30,000 and 40,000 monitoring points by each radar unit. The locations of the center points of the pixels

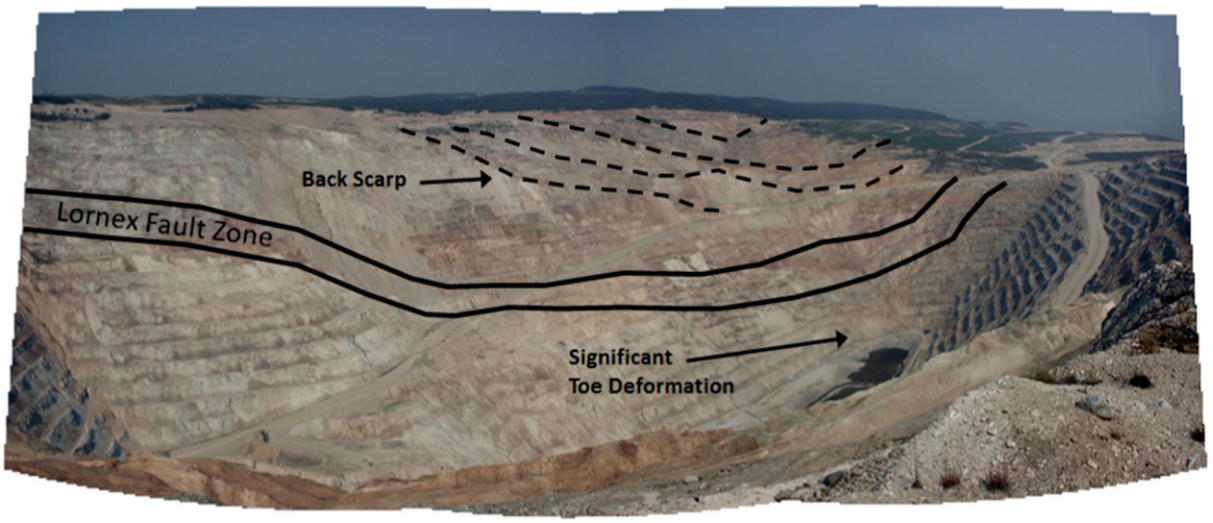

Fig. 2. West wall of the Lornex Pit at the Teck Highland Valley Copper mine, showing the location of the Lornex Fault Zone, and graben-like backscarps and toe bulging that has developed with pit wall movements.

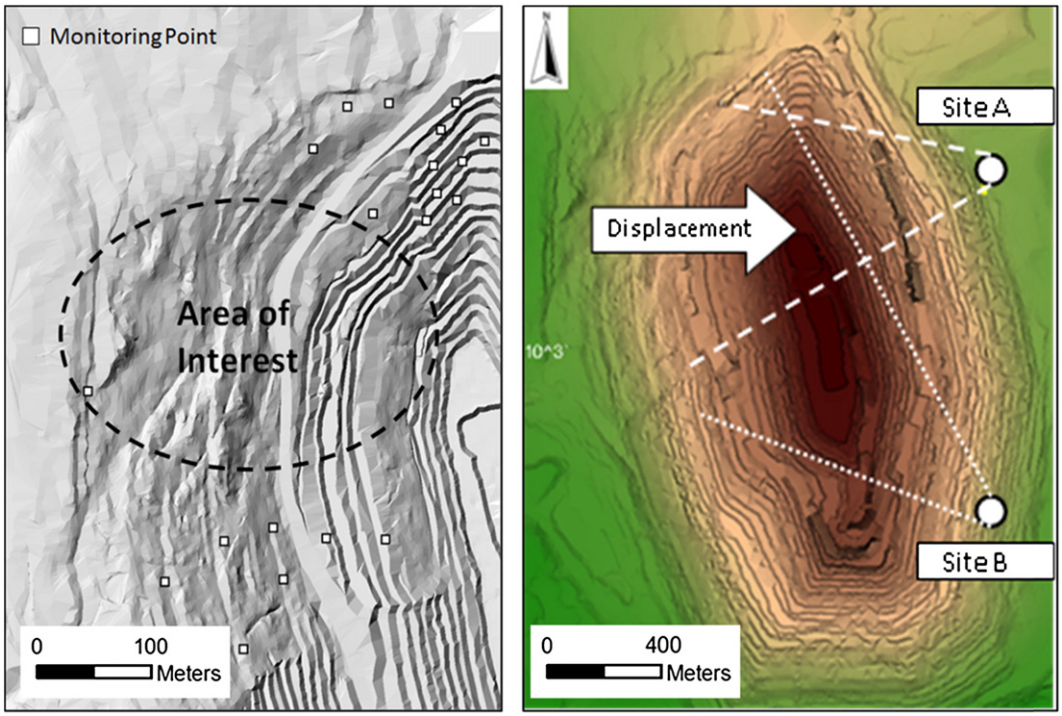

Fig. 3. Location of geodetic operational prisms on the northwest wall Lornex (left) and the IBIS-M radar monitoring sites (right) with respect to the portion of the wall undergoing the highest rates of displacement (within dashed lines).

Fig. 4. Site preparation and installation of the IBIS-M radar unit for the 3-D radar experiment, showing: leveling and grading of gravel site pad, lifting of concrete filled drums for radar base, fitting of leveled radar guide rail, and radar positioning for pit wall monitoring.

were compared and matched, and approximately 25,700 points were found to be common between the two data sets.

Based on the original location common to each raster set (X_{A1},Y_{A1}, $Z_{A1} = X_{B1}$,Y_{B1},Z_{B1}), the corresponding line-of-sight displacement magnitude and the location of each radar instrument, a displacement vector for each direction of movement was created (X_{A2},Y_{A2},Z_{A2} and X_{B2},Y_{B2}, Z_{B2}) using the formula:

$$(x_2, y_2, z_2) = (x_1, y_1, z_1) + R * [(x_1, y_1, z_1) - (x_o, y_o, z_o)] \quad (1)$$

where x_o,y_o,z_o is the instrument location, and R is the ratio of the measured displacement and distance from the instrument.

For each of the new vectors created, the equation of the plane perpendicular to that vector at the new point (X_{A2},Y_{A2},Z_{A2} and X_{B2},Y_{B2},Z_{B2}) was determined. The actual displacement of each raster cell must exist on both planes; therefore, the end of the combined displacement vector exists on the line created by the intersection of these two planes.

In the absence of a third radar unit to allow for true 3-D triangulation, one of the values of the new vector was assumed. In this case, an estimated value for the elevation was evaluated by using two techniques: an average Z value and a weighted Z value based on displacement. For the weighted Z value, the elevation of the new vector was determined using the following relationship:

$$\frac{\text{Displacement A}}{\text{Displacement B}} \approx \frac{\Delta Z_A}{\Delta Z_B}. \quad (2)$$

Inspection of the results using this relationship suggested that the weighted Z value (i.e., weighted elevation values) produced a unique solution for the combined A + B vectors (X_{Comb},Y_{Comb},Z_{Comb}).

An idealized example is shown in Fig. 5. In this example, two vectors are created from the respective line-of-sight displacements (Sites A and B) with corresponding planes perpendicular to the vectors. The two planes are plotted with a resultant line of intersection.

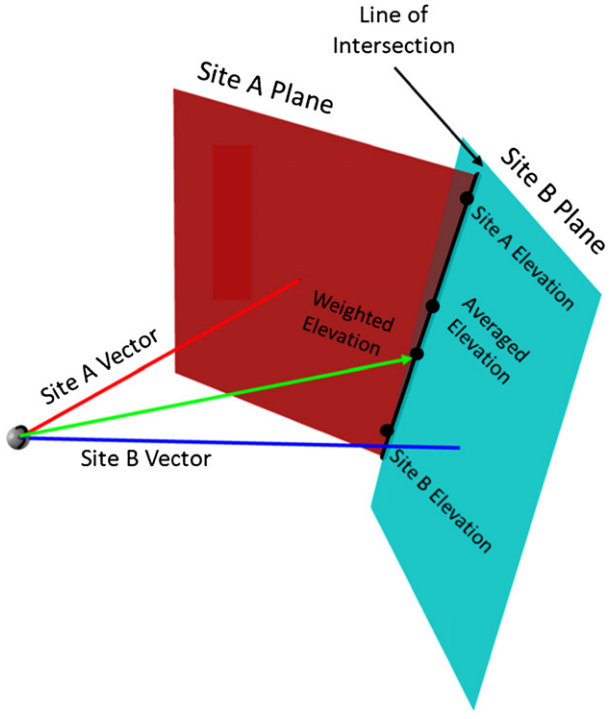

Fig. 5. Determination of pseudo-3D vector (green) resolved from the line-of-sight vectors (A and B) and a weighted elevation assumption along the line of intersection between planes normal to A and B. Also shown is the average elevation option.

For a given elevation value entered into the equation representing the line of intersection, both X and Y values can then be determined. In this case, when a larger amount of displacement is recorded by one instrument, it is assumed that the direction of movement for that cell is more similar to the direction parallel to the line of sight of that instrument and a weighted value for the elevation (Eq. (2)) is used. In individual cases, geological features such as the fault or joints can be used to help interpret the direction of movement; however, these assumptions would not be able to be used over the entirety of thousands of points making up the displacement map. Caution should be used when trying to apply specific knowledge to the displacement map as the precise location of the vector and the digital elevation model may lead to the interpretation of an incorrect structure.

4.2. Displacement map generation

The newly created vectors and corresponding points were imported into the CAD software Rhino© (Rhino Software, 2010), and sorted by magnitude. These points/vectors were then draped over a DEM of the Lornex Pit and the Lornex Fault Zone to determine the patterns of movement. Displacement maps based on the individual instruments (Sites A and B) were also created for individual comparison. Unfortunately, no geodetic prisms were operational at the time of the experiment to help calibrate the creation of the 3D displacement map (as seen in Figure 3, left). A further validation experiment was not attempted as the condition of the prisms was not disclosed at the time of the experiment.

4.3. Potential sources of error

Several potential sources of error during the creation of these maps were identified. Rounding errors may be introduced as the CAD software used is able to handle up to 8 significant digits. This error is expected to only be significant where very small displacements are recorded.

In order to create a true 3-D displacement map, three radar units would be required; however, with the use of two units, a pseudo-3D map can be produced. The result of the combination of the two vectors created from each individual unit is the equation of the line of intersection of the two planes. Therefore, the end displacement vector direction can be influenced by the end elevation assumed. If the displacements in the pit wall were predominantly vertical, a larger source of error would be incorporated in the vector direction. In this case, the two radar units were placed at roughly equal elevations and the direction of suspected movement was largely horizontal, meaning that the methods for determining the end elevation did not greatly influence the direction of the vector. If the direction of movement is suspected to contain a larger vertical component, then a different configuration of radar placement would have been required.

As both radar units were located near the crest of the opposite slope, a majority of the pit wall being monitored was below the elevation of the instruments. This means that all movements were recorded in near horizontal or an upward line-of-sight direction. The principal direction of movement is expected to be downward and toward the toe of the pit wall; therefore, only a portion of the displacement was resolvable. In order to achieve a more realistic vector, at least one of the instruments should be located nearer to the bottom of the pit; however, this presents logistical and safety problems in an operating mine environment and possible interference with pit operations.

Another potential source of error was the displacement of the monitoring units during the data collection. The end and center points of both units were surveyed at the start, mid-point, and completion of the monitoring period to capture any movement and/or rotation of the radars.

5. Three-dimensional displacement pattern

5.1. Line of sight displacement magnitudes

The pattern of total cumulative displacements observed from Sites A and B during the monitoring period is shown in Fig. 6. At Site A, displacement values ranged between +26 and −220 mm/day, while at Site B, displacement values ranged between +35 and −275 mm/day. Negative values represent movement toward the instrument, while positive values represent movement away from the instrument. For the slope monitored at THVC, movement away from the radar is interpreted as displacement along the graben toppling structures which dip into the slope.

Although the instruments were focused upon the same slope segment, the displacement patterns recorded from Sites A and B were found to be similar with slightly different boundaries and, in some cases, magnitude. This confirms the presence of absolute movement occurring in distinct areas of the pit wall and that the different perspectives of the instrument can capture different components of that movement. The comparison between the two displacement patterns highlights the importance of the investigative processes used in understanding the failure or displacement mechanism within a slope prior to setting thresholds used to set monitoring alarms. If a single (often arbitrary) position is picked for slope monitoring, the nature of the pit wall movement may not be observed.

5.2. Combined displacement magnitudes

The combined displacements measured from the two radar systems lead to the pattern observed in Fig. 7. Displacement values ranged between 0 and 307 mm/day and as much as 750 mm cumulative displacement over the monitored 4 day time period. As the vectors have been combined, displacements no longer have to be referenced as being toward or away from the instruments as in line-of-sight monitoring techniques but rather an absolute value. These results show maximum displacement values that are higher than the 100 mm/day average reported for the geodetic prisms (Rose and Scholz, 2009). Likely explanations for this discrepancy include the large number of points being measured, the opportunity to measure near vertical rock faces and areas moving too rapidly to install stable prisms, and the mining activities at the time of the experiment which may have influenced activity along the LFZ.

By creating the pseudo-3D displacement map, a more complete representation of the location and pattern of displacements in the slope can be achieved. Based on the combined displacement pattern, several distinct zones of displacement can be observed in Fig. 7, including: i) below the Lornex Fault near the base of the pit, ii) just above the LFZ near a former access ramp, and iii) in the upper reaches of the slope. The full extent of these lobes can be determined as well as smaller zones within the pit wall. The zones of concentrated displacements resolved by combining the individual radar line-of-sight displacements highlight several smaller areas of localized displacement otherwise not discernible in either of the individual displacement plots. These displacement zones can then be used, in combination with the conventional geodetic data, to aid the creation of a conceptual model used to interpret the measured displacements and the underlying kinematics of the slope, the limits of movement within the slope, and to help calibrate future 2D and 3D numerical deformation models.

5.3. Displacement vectors

The displacement direction of each monitoring point can be resolved into a vector from the individual sets of radar monitoring data from monitoring sites A and B (Figure 8). The enlarged region in Fig. 8 shows an example of an area with higher displacement rates in the slope. By plotting the displacement vectors, several independent lobes of movement within the slope are observed which are likely controlled by separate structures within the rock mass as well as changes in lithology and constitutive behavior of the rock mass.

The vectors indicate toppling movements in the upper slope above the Lornex Fault, which agrees with the presence of a persistent discontinuity set that dips steeply into the slope.

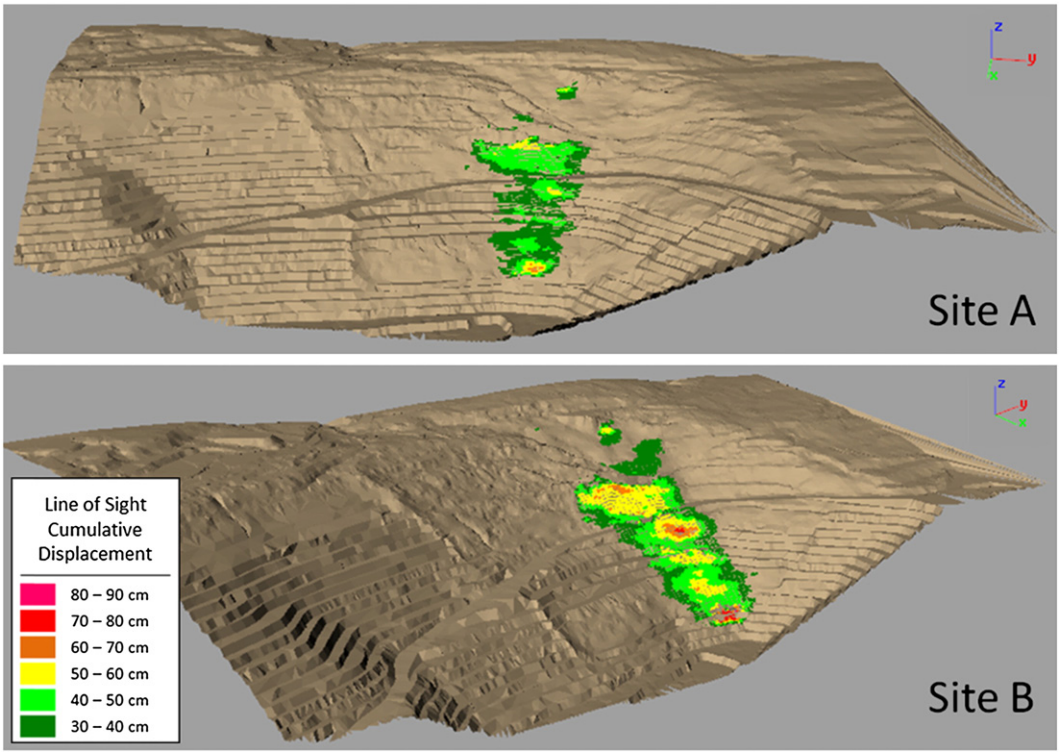

Fig. 6. Radar measured line-of-sight displacement patterns from: a) Site A, and b) Site B.

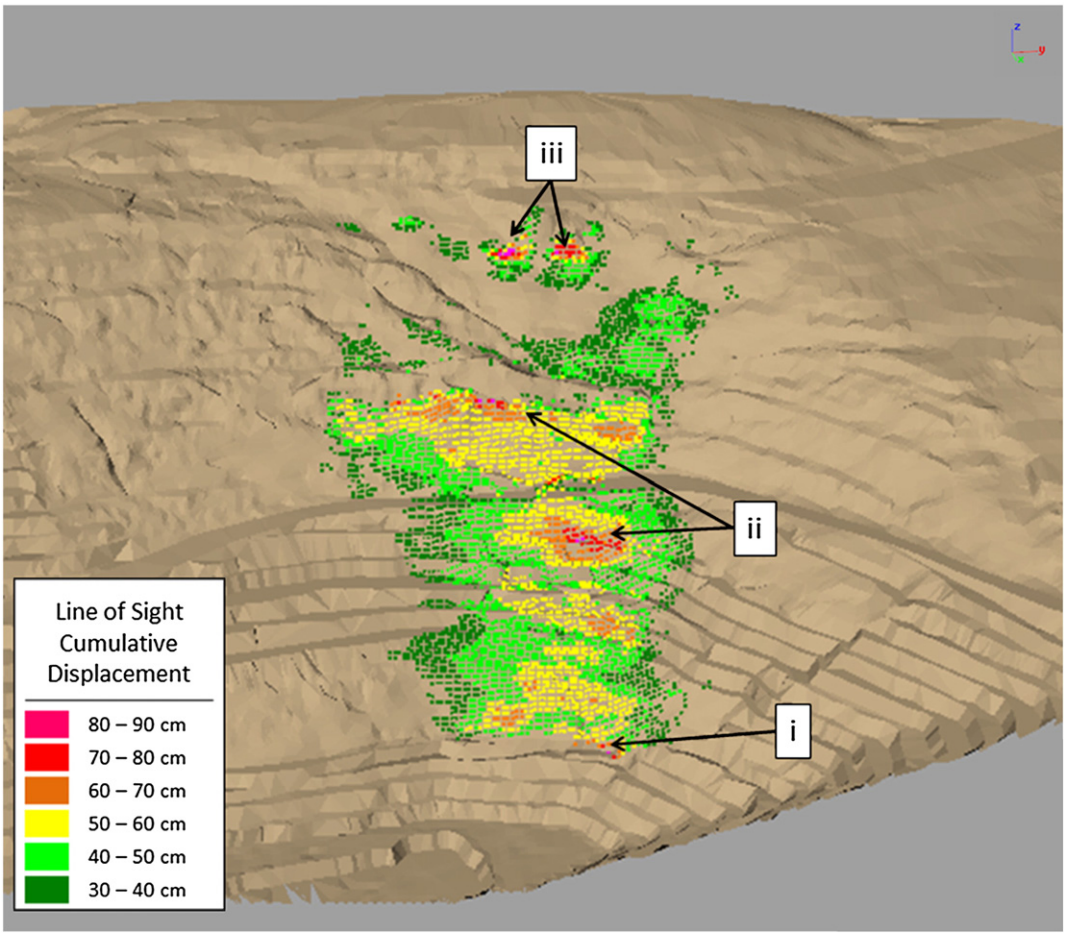

Fig. 7. Combined displacement pattern from Sites A and B. Several distinct zones are identified (i, ii and iii), as described in the text.

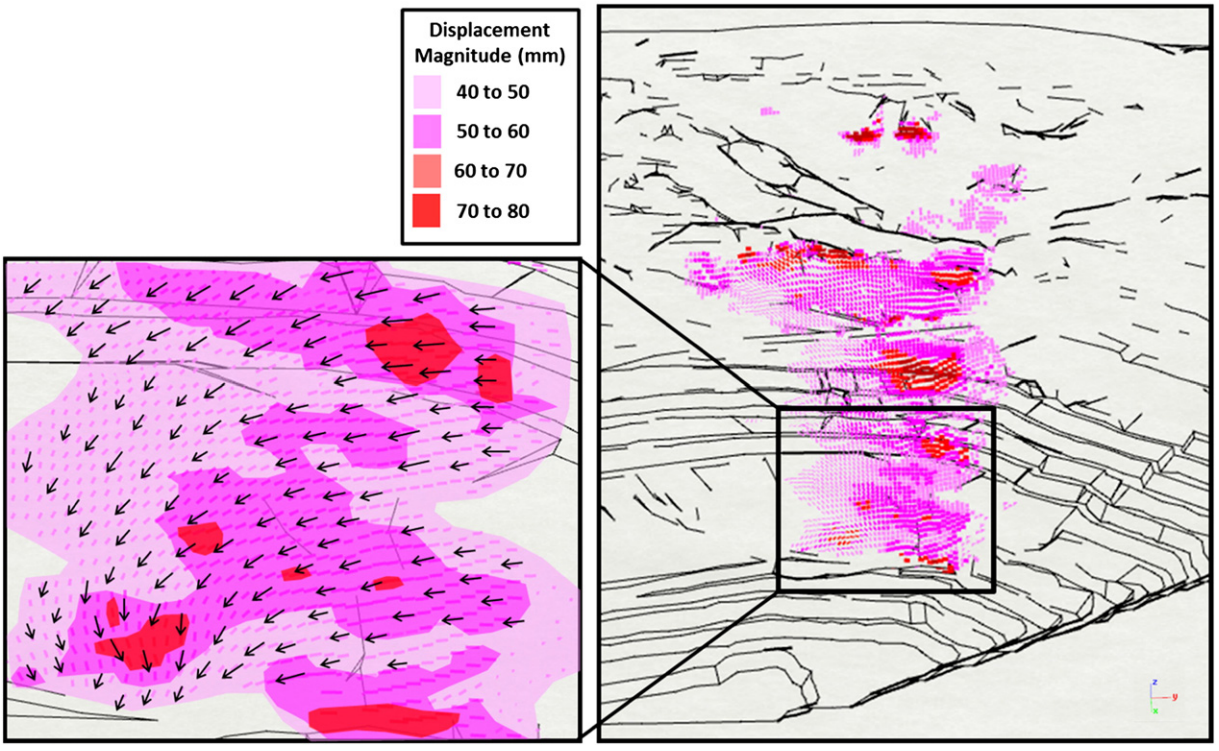

Fig. 8. Combined vector map from Sites A and B, with vectors scaled to displacement magnitudes to show direction of movement. Left diagram shows an enlarged view of the lower slope (approximately 125 × 125 m).

6. Pit slope kinematics

Review of the combined radar displacement data (magnitude, direction, and plunge) allows for an expansion of earlier slope kinematic models (Tosney et al., 2004; Piteau Associates Ltd, 2008; Rose and Scholz, 2009), which were created to describe the observed displacements within the Lornex Pit based on field observations and geodetic data, complemented by 2-D numerical analyses. Fig. 9 shows projections of the 3-D radar data in terms of cumulative displacement magnitude, displacement azimuth and plunge taken directly from the displacement vectors (Figure 9a through c). Each of the aspects of the displacement vectors was reviewed in detail to identify potential failure mechanisms, in particular abrupt changes in the values were concluded to be controlled by structural features within the slope.

A bias within the plunge data exists as the setup locations of both radars were placed near the pit rim, giving rise to an upward plunge in the line of sight displacement. The plunge values should only be used as a tool to help guide in the identification of possible rock displacement kinematics and to determine areas of relative upward movement. Fig. 9d shows the interpreted kinematic modes based on the 3-D radar data, which were then used to develop the engineering geology model of the interpreted pit wall deformation mechanisms in Fig. 10.

Several key observations with respect to displacement patterns and slope kinematics can be observed within the plots in Fig. 9. Within a continuum environment, displacement within the pit arising from the excavation would tend to show a gradual change in magnitude, azimuth and plunge as the rock responds to the changes in stress. The discontinuous nature of the measured displacement indicates that rock mass response can be partially or fully controlled by large scale structures such as faults. Both small variations and abrupt changes can be detected within both the displacement data suggesting not only movement or separation along structures but also yielding of the rock mass in between the faults.

Comparison between the displacement magnitude and azimuth indicates that the areas with the highest total displacement above the Lornex Fault tend to move toward directions between 120° and 150°. Movement within the northwest corner between the Lornex Fault and the pit access ramp is interpreted as being predominantly sliding

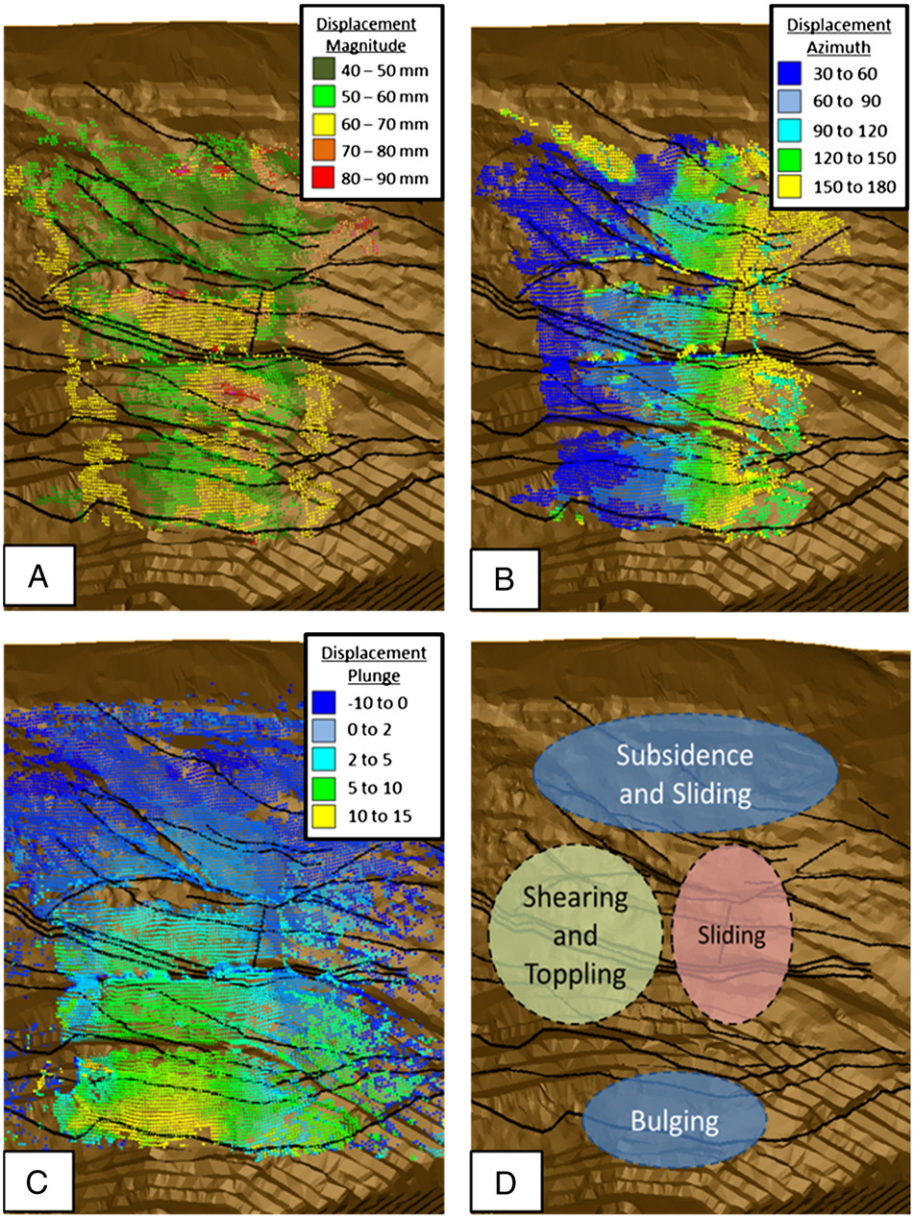

Fig. 9. Oblique view of the northwest corner of the Lornex Pit, highlighting areas of higher displacement (left) and movement directions (right).

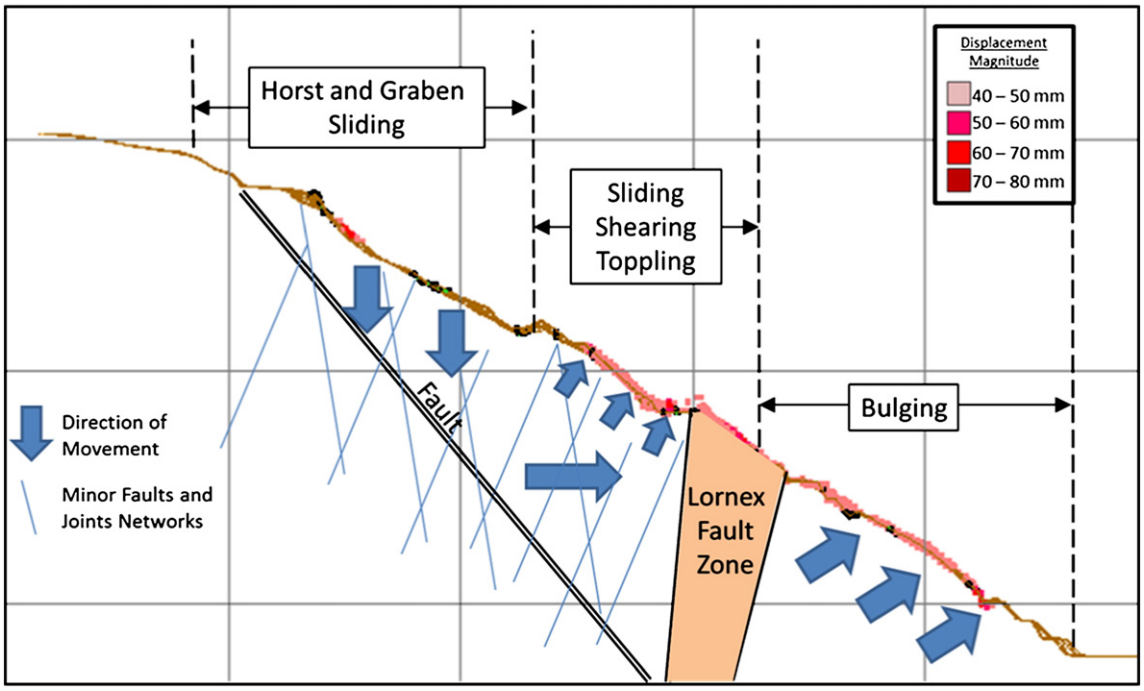

Fig. 10. Schematic diagram of interpreted kinematics for the northwest wall of the Lornex Pit.

controlled by a shallow dipping fault (W1-1) sub-parallel to the slope or shear structures parallel to the W1-1 Fault. The sliding allows for the development of graben-like blocks to form and drop into the space created by the translational sliding (Figure 10). The presence of a basal fault controlling sliding in the upper slope is in agreement with the kinematic model developed by Rose and Scholz (2009). In the western half of the upper slope, these displacements decrease in magnitude and become more sporadic in terms of direction. Together they suggest that the movement within this region is dominated by toppling and shearing of the rock mass induced by the dilation of the rock mass and loss of confinement within the slope. Significant sliding may not be observed within the west wall due to the angle of incidence between the fault and the pit wall. As the pit wall direction curves toward the south, sliding along the fault is enabled.

The lower line of sight displacements within the upper portion of the slope and interpretation that these are being dominated by vertical downward movements of graben-like blocks are supported by geodetic data that exists outside of the area monitored by the experiment. The lack of directional correlation in the 3-D radar data below the LFZ suggests that the rock mass below the fault (altered Skeena Quartz Diorite) is undergoing bulging through shearing and dilation of the rock. Thus the 3-D radar data shows a clear and distinct difference in slope behavior from that of the complex sliding–shearing–toppling mechanism interpreted in the upper slope. This corresponds with the presence of weaker, more tectonically disturbed rock below the Lornex Fault combined with higher shear stresses at the toe of the slope.

7. Conclusions

A novel experiment involving the simultaneous deployment of two ground-based radar systems was conducted to collect continuous, line of sight displacement data in "stereo" of a large, moving open pit slope bisected by a large fault. The simultaneous monitoring with two synthetic aperture radar units has led to the construction of a high resolution, pseudo-3D displacement map of a large open pit rock slope. Analysis of the corresponding displacement vector map allowed an interpretation of the overall slope kinematics to be resolved. The 3-D radar experiment was able to identify localized movements related to smaller-scale geological structures and changes in pit wall slope orientation.

The radar monitoring clearly provided a significant increase in coverage above that possible using geodetic prisms, with over 25,000 common displacement points. The need to extrapolate displacements between prisms is avoided and small areas of high displacement that may pose potential safety concerns can be better identified and monitored. Furthermore, areas which cannot be monitored due to poor or dangerous access can be covered by the radar without the need to install prisms. For the 3-D radar experiment reported here, the monitoring was able to identify localized movements related to smaller-scale geological structures and changes in pit wall slope orientation.

Understanding of the pit slope kinematics was significantly improved through the use of the pseudo 3-D radar data. This has the potential to add significant value to a mine project where the mine plan is considering a pit wall pushback to deepen the pit. In such cases, the influence of the controlling nature of any major faults and smaller structures on the pit wall movements can be investigated and better understood with respect to pit geometry, slope deformation kinematics, evolving failure mechanisms, and ultimately geo-risk. This is the subject of ongoing research, and involves the integration of the 3-D slope deformation map with advanced 3-D numerical modeling. Preliminary modeling using the distinct element code 3DEC has been carried out to further investigate and validate the kinematic model derived from the 3-D radar data. In parallel, the 3-D radar data is being used to calibrate the model with respect to the controlling influence of important fault and joint properties, including location, persistence, and strength characteristics. These can then be projected for future deepening of the pit and pushback of its slopes.

Acknowledgments

The authors would like to thank Teck Highland Valley Copper for providing access to the mine site, logistical support, mine data and financial support for the experiment. Logistical support was also provided by Renato Macciotta and Prof. Derek Martin from the University of Alberta in the setup of the shared radar unit acquired through an NSERC Research Tools and Instruments grant. The authors would also like to

thank IDS Ingegneria Dei Sistemi for personnel and technical support as well as the use of the second IBIS-M radar unit for this experiment. Funding for this experiment was provided by Teck Highland Valley Copper and a British Columbia Innovation Council Natural Resources and Applied Sciences (NRAS-RTP-2009-SFU-026) Endowment grant.

References

Piteau Associates Ltd, 2008. Open pit geotechnical assessments and preliminary slope design criteria for the Lornex Pit L16 Expansion. Intern. Doc.

Brown, N., Kaloustian, S., Roeckle, M., 2007. Monitoring of open pit mines using combined GNSS satellite receivers and robotic total stations. In: Potvin (Ed.), In Proceedings: 2007 International Symposium on Rock Slope Stability in Open Pit Mining and Civil Engineering. ACG, Perth. Perth, pp. 417–429.

Casagli, N., Catani, F., Del Ventisette, C., Luzi, G., 2010. Monitoring, prediction, and early warning using ground-based radar interferometry. Landslides 7 (3), 291–301.

Day, A.P., Seery, J.M., 2007. Monitoring of a large wall failure at Tom Price Iron Ore Mine. In: Potvin (Ed.), In Proceedings: 2007 International Symposium on Rock Slope Stability in Open Pit Mining and Civil Engineering, Perth. ACG, Perth, pp. 333–340.

Di Traglia, F., Intrieri, E., Nolesini, T., Bardi, F., Del Ventisette, C., Ferrigno, F., Frangioni, S., Frodella, W., Gigli, G., Lotti, A., Tacconi Stefanelli, C., Tanteri, L., Leva, D., Casagli, N., 2014. The ground-based InSAR monitoring system at Stromboli volcano: linking changes in displacement rate and intensity of persistent volcanic activity. Bull. Volcanol. vol. 76, 786.

Fukuzono, T., 1985. A new method for predicting the failure time of a slope. In Proceedings: 4th International. Conference and Field Workshop on Landslides. Tokyo University Press, Tokyo, pp. 145–150.

Harries, N.J., Roberts, H., 2007. The use of slope stability radar (SSR) in managing slope instability hazards. In: Eberhardt, et al. (Eds.), Rock Mechanics, Meeting Society's Challenges and Demands. In Proceedings: 1st Canada–US Rock Mechanics Symposium, Vancouver. Taylor & Francis, London, pp. 53–59.

Harries, N., Noon, D., Rowley, K., 2006. Case studies of slope stability radar used in open cut mines. In Proceedings: Stability of Rock Slopes in Open Pit Mining and Civil Engineering Situations, Johannesburg. SAIMM, Johannesburg, pp. 335–342.

Herrera, G., Fernández-Merodo, J.A., Mulas, J., Pastor, M., Luzi, G., Monserrat, O., 2009. A landslide forecasting model using ground based SAR data: the Portalet case study. Eng. Geol. 105 (3), 220–230.

Martino, S., Mazzanti, P., 2014. Integrating geomechanical surveys and remote sensing for sea cliff slope stability analysis: the Mt. Pucci case study (Italy). Nat. Hazards Earth Syst. Sci. 14, 831–848.

Monserrat, O., Moya, J., Luzi, G., Crosetto, M., Gili, J.A., Corominas, J., 2013. Non-interferometric GB-SAR measurement: application to the Vallcebre landslide (eastern Pyrenees, Spain). Nat. Hazards Earth Syst. Sci. 13, 1873–1887.

Moore, D.P., Imrie, A.S., Baker, D.G., 1991. Rockslide risk reduction using monitoring. In Proceedings: Canadian Dam Association Meeting, Whistler, BC. Canadian Dam Safety Association, pp. 245–258.

Noferini, L., Pieraccini, M., Mecatti, D., Macaluso, G., Atzeni, C., Mantovani, M., Tagliavini, F., 2007. Using GB-SAR technique to monitor slow moving landslide. Eng. Geol. 95 (3), 88–98.

Rödelsperger, S., Läufer, G., Gerstenecker, C., Becker, M., 2010. Monitoring of displacements with ground-based microwave interferometry: IBIS-S and IBIS-L. J. Appl. Geodesy 4 (1), 41–54.

Rose, N.D., Hungr, O., 2007. Forecasting potential rock slope failure in open pit mines using the inverse-velocity method. Int. J. Rock Mech. Miner. Sci. 44 (2), 308–320.

Rose, N., Scholz, M., 2009. Analysis of complex deformation behaviour in large open pit mine slopes using the Universal Distinct Element Code (UDEC). In Proceedings: Slope Stability 2009, International Symposium on Rock Slope Stability in Open Pit Mining and Civil Engineering Santiago (CD-ROM, 11 pp.).

Rhino Software, 2010. NURBS Modeling for Windows. McNeel, Seattle.

Talich, M., Glöckner, M., Böhm, O., Antoš, F., Soukup, L., Havrlant, J., Šolc, J., 2014. The application of the ground-based InSAR technique for the deformation monitoring of concrete hydropower dam Orlík on Vltava River. INGEO 2014 — 6th International Conference on Engineering Surveying, Prague, Czech Republic, April 3–4, 2014.

Tarchi, D., Casagli, N., Fanti, R., Leva, D.D., Luzi, G., Pasuto, A., Silvano, S., 2003. Landslide monitoring by using ground-based SAR interferometry: an example of application to the Tessina landslide in Italy. Eng. Geol. 68 (1), 15–30.

Farina, P., Leoni, L., Babboni, F., Coppi, F., Mayer, L., Coli, N., Thompson, C., 2012. Monitoring engineered and natural slopes by ground-based radar: methodology, data processing and case studies review. In Proceedings: SHIRMS 2012. SAIMM, p. 10.

Tosney, J.R., Milne, D., Chance, A.V., Amon, F., 2004. Verification of a large scale slope instability mechanism at Highland Valley Copper. Int. J. Surf. Min., Reclam. Environ. 2004 18 (4), 273–288.

Walker, P., Knight, P., Johnson, T., Speight, H., 2006. Pushback 8 South — a case study in pit slope management. In Proceedings: Stability of Rock Slopes in Open Pit Mining and Civil Engineering Situations, Johannesburg. SAIMM, Johannesburg, pp. 435–450.

Willenberg, H., Evans, K., Eberhardt, E., Spillmann, T., Loew, S., 2008. Internal structure and deformation of an unstable crystalline rock mass above Randa (Switzerland): Part II — three dimension deformational patterns. Eng. Geol. 101 (1–2), 15–32.